JVSTA
JOURNAL OF VACUUM SCIENCE AND TECHNOLOGY A

Comparison endpoint study of process plasma and secondary electron beam exciter optical emission spectroscopy

P. L. Stephan Thamban, Stuart Yun, Gabriel Padron-Wells, Jimmy W. Hosch, and Matthew J. Goeckner

Citation: J. Vac. Sci. Technol. A **30**, 061303 (2012); doi: 10.1116/1.4756694
View online: http://dx.doi.org/10.1116/1.4756694
View Table of Contents: http://avspublications.org/resource/1/JVTAD6/v30/i6
Published by the AVS: Science & Technology of Materials, Interfaces, and Processing

Comparison endpoint study of process plasma and secondary electron beam exciter optical emission spectroscopy

P. L. Stephan Thamban[a] and Stuart Yun
Department of Mechanical Engineering, The University of Texas at Dallas, 800W Campbell Road, Richardson, Texas 75080

Gabriel Padron-Wells
Department of Electrical Engineering, The University of Texas at Dallas, 800W Campbell Road, Richardson, Texas 75080

Jimmy W. Hosch
Verity Instruments, Inc., 2901 Eisenhower Street, Carrollton, Texas 75007

Matthew J. Goeckner
Department of Mathematical Sciences, The University of Texas at Dallas, 800 W Campbell Road, Richardson, Texas 75080

(Received 4 May 2012; accepted 17 September 2012; published 3 October 2012)

Traditionally process plasmas are often studied and monitored by optical emission spectroscopy. Here, the authors compare experimental measurements from a secondary electron beam excitation and direct process plasma excitation to discuss and illustrate its distinctiveness in the study of process plasmas. They present results that show excitations of etch process effluents in a SF_6 discharge and endpoint detection capabilities in dark plasma process conditions. In SF_6 discharges, a band around 300 nm, not visible in process emission, is observed and it can serve as a good indicator of etch product emission during polysilicon etches. Based on prior work reported in literature the authors believe this band is due to SiF_4 gas phase species. © *2012 American Vacuum Society*. [http://dx.doi.org/10.1116/1.4756694]

I. INTRODUCTION

For several decades, direct optical emission spectroscopy, OES, signals have been central to process control for plasmas.[1–3] As feature sizes have reached the low-nanometer regime, processing steps have been moved to either low power or remote plasma conditions to minimize ion induced damage and maintain the integrity of the features.[4] In such situations, light emission above the wafer is minimal and direct OES signal-to-noise ratio (SNR) becomes poor. Moreover, for many of these low-nanometer devices, only "small open areas," e.g., small percentage of the wafer, are processed in many steps. This combination of poor SNR and low percentage open area pose a serious challenge to traditional process control schemes such as end point detection with OES signals.

To overcome some of the limitations in traditional direct OES control, we have developed a new diagnostic system[5] that relies on a secondary excitation, electron beam. The novelty in this method is that a controllable electron beam, e-beam, is used to excite gas species to fluorescence. In fact, this controlled e-beam provides one with the ability to excite species in ways till now not accessible with traditional plasma excitation. In this paper, we describe measurements conducted with the e-beam OES method during polysilicon etch experiments with SF_6 discharges. Specifically, we examine SF_6 plasmas in our modified gaseous electronics conference (mGEC) tool.[6] SF_6 discharges were chosen for this study because they are commonly used in numerous applications such as the Bosch process[7] and other Si etch systems.[8–12] However, due to the electronegative[13] nature of the discharge, the electron density in the plasma tends to be low and thus the emission intensities are weak. Under such conditions, process control schemes such as endpoint detection can be a difficult task.

In this paper, we monitored processes using our new e-beam diagnostic and two more traditional gas chemistry diagnostics tools, direct OES and Fourier transform infrared (FTIR) spectroscopy. In Sec. II, we describe the experimental setup, noting some of the strengths and weakness of each of the diagnostic tools. In Sec. III, we present the results and discuss the implications. In Sec. IV, we summarize.

II. EXPERIMENT

The reactor used in these studies was a mGEC reactor cell, see Fig. 1.[14,15] In this reactor, the RF source coil configuration is similar to that of a standard inductively coupled plasma (ICP) GEC reference cell reactor.[16,17] The water cooled rf coil has planar geometry with five turns. It is powered at the center and grounded on the outside turn. The mGEC system is different from the GEC in that the source to chuck gap can be smoothly varied between 2 and 17 cm, while the effective chamber diameter can be 20, 40, 60, or 66 cm. Such a design provides a unique merit in which it allows control over the ion flux to the process wafer placed on the chuck and wall interactions. In this study, we employed the 60 cm diameter wall for all the measurements. The source to chuck gap was set at various positions, so as to mimic modern remote plasma systems. A 13.56 MHz Daihen RF generator, Model# DRFS-10SB, was used to supply RF

[a]Electronic mail: stephan@utdallas.edu

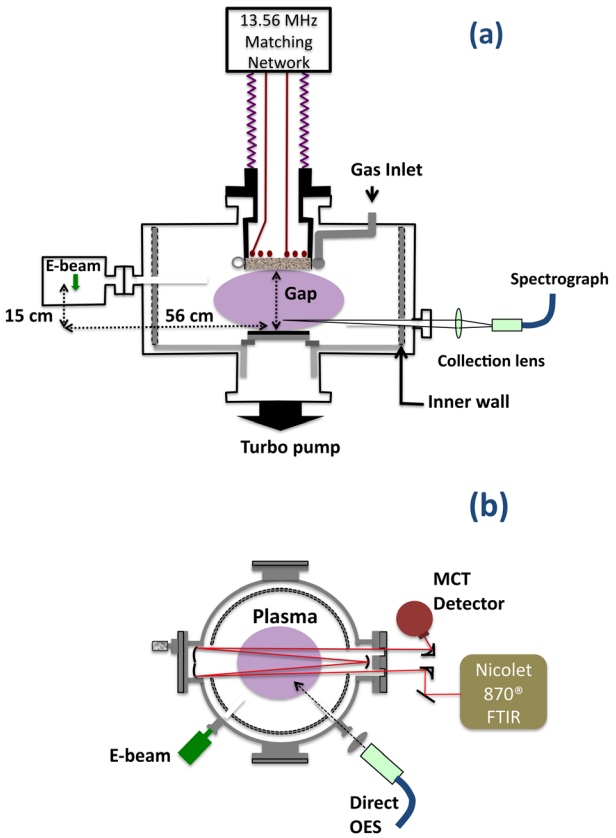

FIG. 1. (Color online) (a) mGEC ICP, gas flow, and inner wall configuration schematic. Inner wall radius was held fixed at 30 cm but source to chuck gap could be varied between 2 and 17 cm. Direction of e-beam in the sensor is indicated by the block arrow. (b) Schematic of diagnostics in mGEC reactor. Access ports through which process gas phase measurements were conducted with the three diagnostics, electron beam (e-beam) system, direct-OES, and FTIR spectroscopy are shown.

power to the plasma, while the wafer substrate was not powered in these experiments.

The base pressure in the chamber was in the 10^{-6} Torr range and pressure in the chamber could be regulated with a throttle valve. Process gas was administered into the chamber through a perforated annular tube around a ceramic RF dielectric widow. SF_6 flow rate was set between 7 and 15 SCCM during experiments. Such low flow rates and the pressure (20, 40 mTorr) chosen during the experiments in this large volume reactor (~100 l) provided a long residence time, ~21 s, condition during experiments.

Direct light emission of the process plasma at a distance 0.25 in. above the wafer was collected using UV grade biconvex lens and fiber optic assembly. It was analyzed using a Verity Instruments SD1024D spectrograph, with a spectral resolution of 1.7 nm. Assuming electron impact excitations in plasmas direct OES emission intensities can be analytically described as

$$I(\lambda) = n_g K_D(\lambda) \int_0^\infty Q\sigma_\lambda(v) v f_e(v) 4\pi v^2 dv, \tag{1}$$

where n_g is the gas density, $K_D(\lambda)$ is the detector sensitivity at the wavelength λ, Q is quantum yield for emission, σ_λ is the optical excitation cross section of the species for that emission wavelength, and f_e is the electron velocity (or energy) distribution function (EEDF). This relation has been exploited in the measurement technique known as actinometry.[18] In actinometry, a small, known amount of inert gas referred as actinomer is introduced along with the process gas and a normalized intensity measurement provides species density information. The density of a species of interest whose emission line intensity, $I(\lambda_s)$, is therefore given as

$$n_s = \frac{n_a I(\lambda_s)}{I(\lambda_a)}, \tag{2}$$

where n_a is the known actinomer density, $I(\lambda_a)$ is the emission line intensity of a specific transition of the actinomer, and k is proportionality constant. This constant is set by the detector sensitivity ratios, optical excitation cross section ratios, and the quantum yield ratios. The above relation holds true only if the threshold energy and the optical excitation cross section function of the transitions considered are similar over the range of energies of the electrons present in the region of interest.

It is evident that to use Eq. (1) in direct OES analysis, a fundamental limitation, that is the lack of knowledge of the process plasma EEDF, particularly the high-energy component, exists. Without this knowledge, quantitative estimates of species densities are impossible. Nonetheless, direct OES is a powerful measurement to study the temporal evolution of species in a noninvasive way. This is because the radiative lifetimes of excited states of many species is on the order of 10 ns and thus, even with nominally sensitive detectors emitted photons can provide information of the plasma gas phase in real time. We have employed direct OES to monitor gas phase variations during etch end point periods.

FTIR measurements were made with a Nicolet Nexus 870® FTIR system with a multipass White Cell.[14] This setup is effectively identical to that reported in other studies by our group.[6,14,15] Employing liquid nitrogen cooled Mercury Cadmium Telluride detector, infrared absorption due to gas phase species could be measured in the 4000 to 650 cm^{-1} wave number range. This multipass system allowed us to significantly enhance the SNR. In our experiments, we used a four-pass configuration with a total beam path length of 325 cm. Infrared absorption measurements over such a wideband inherently have some measurement time limitation, but it can be close to real time.[19] Because we were seeking better density measurements, we choose to make these measurements over ~15 s. The density measurements were made using Beer's law[20]

$$A(\lambda) = n_g l \sigma = -\ln\left(\frac{I}{I_0}\right), \tag{3}$$

where A is the experimentally measured absorbance[21] at a specific wavenumber, n_g is the species density, l is the path length of the infrared beam through the absorbing medium, and σ is the absorption cross section. I_0 and I are the incident and transmitted intensities, respectively.

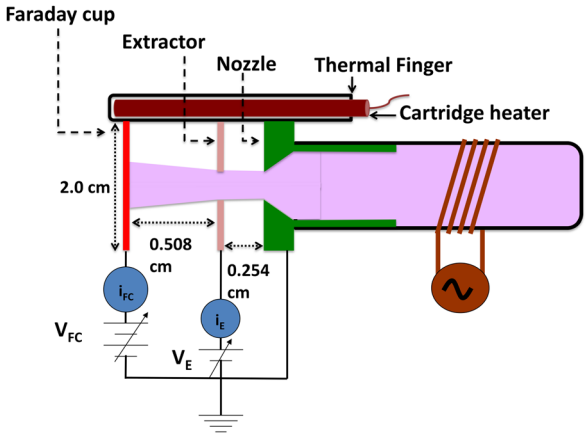

FIG. 2. (Color online) Schematic of the e-beam system. The nozzle electrode opening diameter was 0.254 cm and the extractor electrode opening diameter was 0.508 cm.

The schematic of the e-beam OES is shown in Fig. 2. Plasma generated in a quartz tube with 1.1 cm inner diameter served as an electron source. While other electron sources could conceivably be used (a hollow cathode source was initially studied), our choice of an ICP was to ensure stable functionality of the source in low-pressure (<50 mTorr) process chemistry environments and comply with process reactor material compatibility requirements. The source frequency was 37 MHz and the transmitted RF power as measured by standard BIRD elements was in the 6–15 W range. A nozzle electrode held at ground potential with sufficient ion loss area (2.54 cm long cylindrical surface area) and a 0.254 cm diameter opening served as the electron extraction opening from the plasma source. Gas from the process chamber diffused into the quartz tube through the same opening. A 2.1 cm by 2.0 cm rectangular extractor plate (EX) at a distance of 0.254 cm with a 0.508 cm diameter central opening could be held at a positive bias with respect to the nozzle. This electrode served to set the acceleration potential of the extracted electrons. A second similarly biased plate with identical geometry, except it had no opening, was situated 0.508 cm past the extractor was used to collect those electrons. As this second plate can also used to measure the net current through the system, we refer to it as a Faraday cup (FC). The currents measured at the FC during different measurements reported in this paper were in the 2–4 mA range. A weak axial magnetic field (126 G) was set up using a permanent magnet to collimate the electron beam as it emanated from the nozzle and extractor electrodes. In work not presented here, we have measured that most of the electron current pulled from the plasma arrives at the Faraday cup. The extractor collected the remainder of the current. There is no measureable current to other surfaces. To mitigate deposition on electrode surfaces during operation in process chemistries, the electron extraction assembly was heated to ~350 °C. This was achieved by employing a thermal finger, a vacuum-sealed tube that enclosed a 60 W cartridge heater.

Light generated due to impact excitations as electrons traveled between the extractor and Faraday electrodes was collected using UV grade collection optics positioned 90° to the electron beam. The collection optics consisted a biconvex lens and fiber optic fiber bundle coupled to a Verity SD1024FH spectrograph. Spectral measurements from the e-beam were taken using the spectrograph, with a spectral resolution of 1.7 nm. With a 1× magnification of the fiber optic bundle, the light sampling region was 0.10 cm diameter spot along the e-beam.

Given that electron impact excitations is the primary mechanism for excitation in e-beam OES, the emission intensity of a wavelength is given as

$$I(\lambda) = n_g K_D(\lambda) Q \sigma_\lambda \Gamma_e = n_g K_D(\lambda) Q \sigma_\lambda n_e v_e, \quad (4)$$

where ν_e is the velocity of the electron and n_e is the density. ν_e is set by the accelerating bias used to extract the electrons from the plasma source. It is clear that Eq. (4) is just a special case (monoenergetic electrons) of Eq. (1). When employing our inductively coupled plasma as the electron source, we observe a small spread (~<2 eV, depending on pressure, gas) in the electron energy distribution, while the extractor electrode sets the mean electron energy. For this study, the electron drift energy was set at 190 eV, approximately the peak cross section energy for atomic fluorine. Other energies are possible and may result in stronger signals from the e-beam OES system for some chemical species. The location of the e-beam with respect to the wafer center (origin) was at radial distance of 56 cm and at an axial height of 15 cm, Fig. 1. It is noted that in other experiments[22] and those that will be reported elsewhere, the e-beam system had been successfully employed in other research reactors for measurements of gas phase species and cross-section measurements in our laboratory.

All material samples used in the studies reported below were deposited or grown on 100 mm diameter ⟨100⟩ silicon wafers in the UTD cleanroom. The samples consisted of the base silicon substrate on which a 100 nm thick silicon oxide layer was thermally grown in a Tystar atmospheric furnace. Polysilicon layers of ~1.0 μm thicknesses were deposited via low-pressure chemical vapor deposition (LPCVD) in a Tystar LPCVD tool. Thicknesses of the layers were measured using spectroscopic reflectometry employing a NanoSpec 6100 measurement system. Uniformity of the deposition process across the wafer was verified by measuring thickness at five points on the wafer. It was found to be better than 5% for all the wafers used in the study. These wafers were cleaved into small samples of fixed dimensions to conduct simulated small open area etch experiments. During the processing, the samples were placed directly on the chuck. The simulated resist patterned wafer was approximated as the area of the sample divided by the total area of a 100 mm diameter wafer.

III. RESULTS AND DISCUSSION

A. Emission due to etch effluent, SiF_4

A major factor in our studies was the ability to observe the molecular emission due to SiF_4, distinctly in e-beam OES. This same emission is not observable in direct OES.

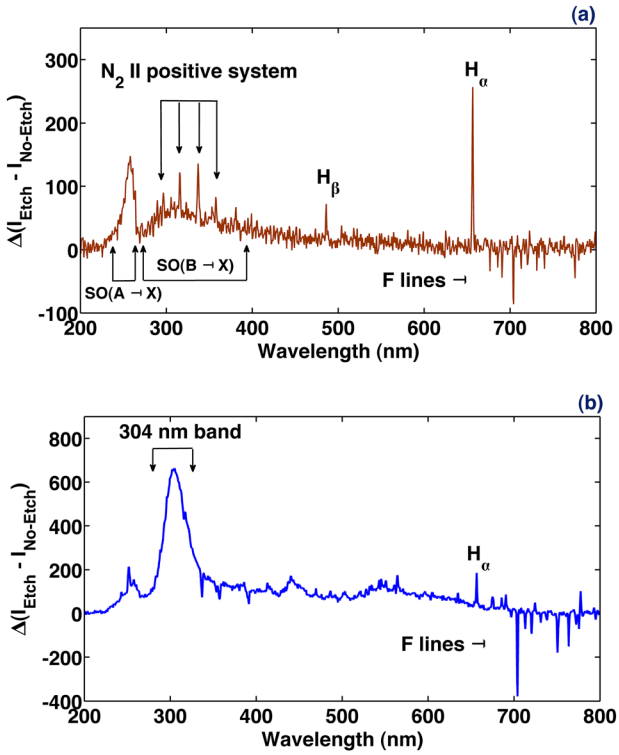

FIG. 3. (Color online) (a) Spectral intensity difference in the 200–800 nm wavelength range between etch (with silicon wafer on the chuck) and no-etch condition measured with direct OES. Prominent molecular emissions (SO, N_2) and atomic emissions (H, F) are shown. (b) Similar difference spectra as measured with e-beam OES. Prominent band at 304 nm (due to SiF_4) and atomic emissions (H, F) are shown.

Utilizing this emission band due to SiF_4, later we will show that etch endpoint results are possible even during low power, low area, and remotely sourced polysilicon etch processes. In Figs. 3(a) and 3(b), difference OES spectra between etch condition (SF_6 discharge and wafer on substrate) and no etch condition (SF_6 discharge and no wafer on substrate) measured directly observing the process emission and using the e-beam diagnostic system are shown. These plots provide an overview of the major chemistry variations in gas phase during a typical polysilicon etch process as measured by the two different OES.

In direct OES, the dominant variation, Fig. 3(a), is observed with fluorine lines in the 680–800 nm range, primarily with the 704 nm F emission line. Other major lines and bands observed in Fig. 3(a) are contributions from contaminants. Trace contaminants, primarily adsorbed water and nitrogen, present in the chamber and process gas are excited in the discharge so Balmer lines of hydrogen ($H_\alpha = 656$ nm and $H_\beta = 486$ nm), second positive system of nitrogen, and its reaction products such as sulfur monoxide[23] (band at 258 and 320 nm) are clearly seen in the difference spectra. Such reactions with contaminants

$$SF_4 + H_2O \rightarrow SOF_2 + 2HF,$$
$$SF_5 + OH \rightarrow SOF_4 + HF,$$

have been reported before[24] in SF_6 discharges. Presence of these contaminants is further confirmed by reaction products such as SOF_2 and HF, which was measured through FTIR measurements. The walls of the mGEC chamber were not heated and contributions due to water desorbing from walls is well known, having been observed to minimize with time by Goeckner *et al.*[25]

In the e-beam difference spectra, Fig. 3(b), a prominent band around 300 nm was observed. The extractor and FC biases were set at 180 and 190 V, respectively, during measurements. Aarts[26] has reported an emission band around 300 nm in his electron impact studies with SiF_4. The UV band with a maximum at 304 nm was measured at electron impact energy of 200 eV. It has also been reported in photo-excitation experiments that SiF_4 can undergo dissociative excitation[27] resulting in an emission band around 304 nm. Clearly the band we observed at 304 nm had strong correspondence with the UV bands of SiF_4 reported in those studies. In Fig. 4(a), we show the integrated intensity trend of the 290–323 nm band during a polysilicon etch process. The polysilicon sample wafer segment used in the measurement had a 15% area with respect to a 100 mm diameter wafer area. Simultaneous FTIR measurements were taken during that experiment. In Fig. 4(b), absorbance band at 1031 cm^{-1} corresponding to SiF_4 is shown. As we show below, the timing and relative changes in strength of those signals are effectively identical. IR spectra taken at four different instances during the etch process are shown. While the e-beam OES measurement was a real-time measurement with an integration period of 100 ms, the FTIR measurement is a time-averaged measurement from multiple scans over a period of

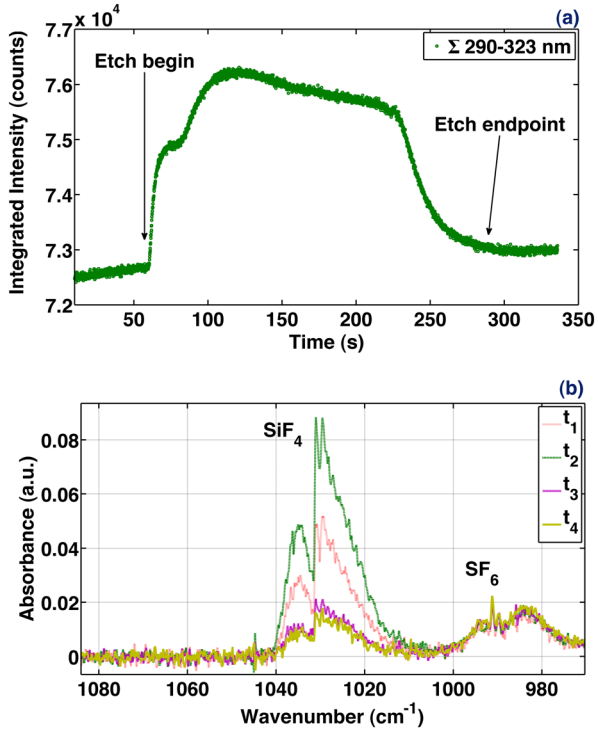

FIG. 4. (Color online) (a) Integrated intensity (290–323 nm) trend due to SiF_4 during a polysilicon etch process. Etch begin and endpoint are shown in the diagram. (b) SiF_4 absorbance band as measured with FTIR spectroscopy at four instances ($t_1 < t_2 < t_3 < t_4$) during the same polysilicon etch process.

~14 s. It is seen that with increasing time from t_1 to t_4, the absorbance signal, thereby the density of SiF_4 increased and eventually dropped at etch endpoint. The calculated densities of SiF_4 at t_1, t_2, t_3, and t_4 were $3.7 \times 10^{13}\,cm^{-3}$, $6.7 \times 10^{13}\,cm^{-3}$, $2.1 \times 10^{13}\,cm^{-3}$, and $1.6 \times 10^{13}\,cm^{-3}$, respectively. Clearly, we find that the integrated intensity trend of the 304 nm band shows a similar trend. Wagner and Brandt[28] have reported with mass spectrometric measurements that the main silicon containing effluent during the etch process in a SF_6 discharge is SiF_4. Moreover given that SiF_4 is a stable effluent during silicon etches, we assign the emission band seen at 304 nm to be that due to SiF_4. While there can be some ambiguity about whether the actual emitting species is excited SiF_3 due to electron impact dissociative excitation as suggested by Suto *et al.*[27] or SiF_4^+ as mentioned in the work of Rosenberg *et al.*,[29,30] in our discussions in this paper we have just considered the parent SiF_4 process effluent that is measured by e-beam OES. Biehl *et al.*[31] have added clarity to that discussion and given that our electron drift energy was set to 190 eV, it strongly suggests that we are measuring the decay due to SiF_4^+.

Since the early days of silicon dry etching using fluorine compounds, SiF_4 is a well known volatile by-product of the etch reaction given as

$$\mathrm{Si\,(solid) + 4F\,(gas) \rightarrow\ SiF_4(gas).}$$

So it is not surprising that it is a species that can clearly indicate silicon etch endpoint. To our knowledge, there are no known reports of OES measurements during etch processes where SiF_4 was monitored. Here, we would like to emphasize one of the important distinctions that an e-beam diagnostic system brings to process studies and process control—the ability to tune the electron impact energies to excite specific species in the gas phase. Aarts[26] has measured threshold for excitation of the 304 nm SiF_4 band to be 21 eV. This provides the reason why the band was not visible in direct OES. For process plasma such as SF_6, typical electron temperature values are between 2 and 5 eV. Assuming an electron distribution that is Maxwellian, it is understandable that the high-energy electron population will be considerably lower. In contrast, we had set the electron impact energy to be 190 eV for most of the e-beam measurements reported in this paper.

In discussions in Sec. III B, we present results from polysilicon etch studies as examined using the 304 nm band with the e-beam OES and the 704 nm emission line trends of direct OES.

B. Endpoint detection in low area, low power, and remote process condition

In this section, we present experimental results that show the endpoint detection capability of the secondary e-beam OES in processes where direct OES SNR is poor. These processes, which were remote (process plasma source to chuck gap is large), low power (60 W), and low etch-area (<5% of a 100 mm diameter wafer area) were studied with both OES methods. In addition, FTIR measurements were made to estimate species densities. Dependencies of OES endpoint results with respect to chuck to source gap variations and etch area variations were experimentally studied. Based on those results a process condition was chosen to run the experiment where the SNR of direct OES is poor and comparatively study the sensitivity of the e-beam OES to detect end point.

Polysilicon etches were conducted with a SF_6 discharge at different source to chuck gaps. Process pressure and power were kept constant at 40 mTorr and 200 W, respectively, in these experiments. The wafer sample had a 1.0 μm thick polysilicon layer above a 100 nm thick SiO_2 layer. The process was chosen with no bias on the chuck to selectively etch the polysilicon layer over the SiO_2 and realize endpoint when etch reached the SiO_2 layer. Also, to have a preferentially lower oxide etch rate, the chuck temperature was set at 15 °C. Wafer samples used in these studies were approximately 4 cm^2 or 5% of the area of a 100 mm diameter wafer area. Noting that the mGEC chamber is large enough to handle 200 or 300 mm wafers, this would be equivalent to ~1% and ~0.5% open areas on standard commercial wafers. In Fig. 5(a), endpoint results measured with the e-beam OES are shown. From these measurements, it is evident that the etch rate decreased as the gap increased. Two scenarios can cause the decrease in etch rate. As the source to chuck gap is increased, ion flux to the surface decreases. This is due to diffusion loss to the walls/surfaces and recombination.[19] Moreover as the source is moved away from the chuck, the high-density region of the plasma gets receded and fluorine density to chuck reduces. This has been experimentally measured through actinometry measurements in C_4F_8 discharges in the mGEC reactor.[19] We expect similar results in SF_6 discharge. Both the decrease in ion flux and reduction in fluorine density should contribute to a decrease in the etch rate. When the etch rate increases, the SiF_4 signal intensity also shows a slight increase. Simultaneous FTIR measurements were made every 30 s during the 10 cm and 12 cm gap experiments and density of SiF_4 as calculated from the absorbance measurements are plotted in Fig. 5(b). The constancy of the SiF_4 density during the process and the loss of the same are seen in the data. It is noticed that time integrated signals versus gap for both the e-beam and FTIR, a weak measure of total SiF_4 produced, are not constant. This may be due to the chemical pathway for production and loss of the SiF_4 and the availability of appropriate species in the system.[19] Understanding this will require further studies. To compare to the e-beam and FTIR results, we also took simultaneous direct OES measurements, see Fig. 5(c). It is observed that the SNR of the direct OES deteriorated as the source to chuck gap increased. (The process discharge exhibited flickering during the 6 cm gap experiment after the endpoint was reached, which is noticeable in the data.) Since SF_6 discharge is an electronegative discharge, it remains strongly coupled just below the source coil, and as the source is raised, the electron temperature falls off readily just above the wafer that is being etched. Optical excitations due to electron impact therefore get diminished in direct OES. Under similar conditions, we find that the target species density, here SiF_4, primarily dictates the SNR of the e-beam OES and that it remains largely unaffected in these measurements.

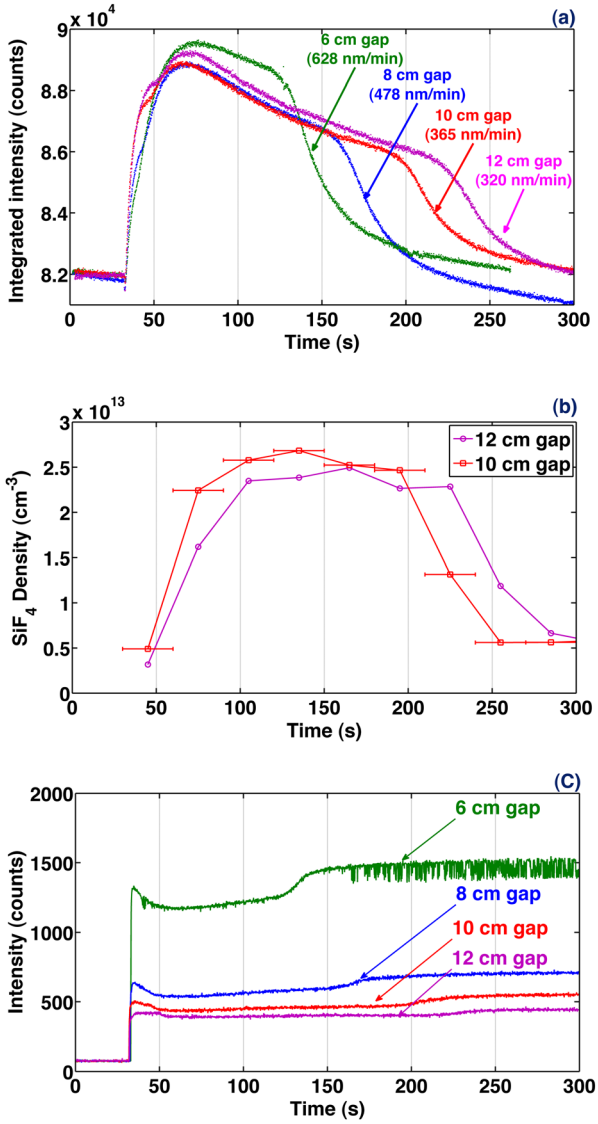

FIG. 5. (Color online) Polysilicon etch processes (200 W process power with SF_6 at 40 mTorr pressure) with 5% area sample at different source to chuck gaps. (a) E-beam integrated (290–323 nm) intensity trend. (b) SiF_4 density determined using FTIR absorption measurements during the 10, 12 cm gap experiments. (c) Fluorine emission line (704 nm) trend measured simultaneously with direct OES during the experiments. In the 6 cm gap experiment process plasma flicker was observed after 150 s.

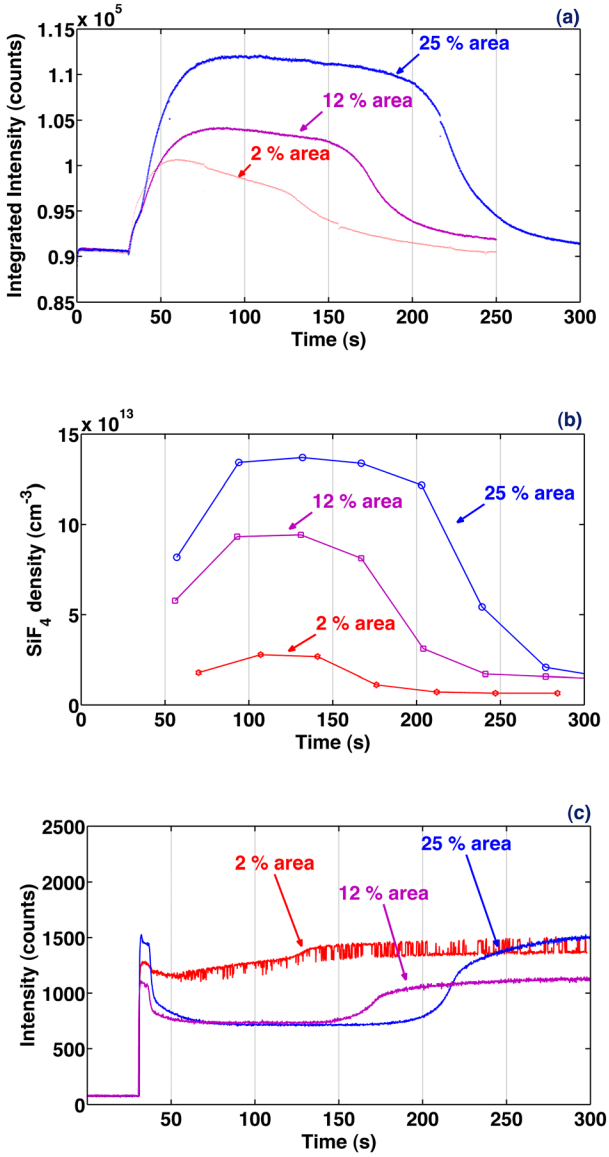

FIG. 6. (Color online) Polysilicon etch processes (200 W process power with SF_6 at 40 mTorr pressure) with 6 cm source to chuck gap for different sample areas. (a) E-beam integrated (290–323 nm) intensity trend. (b) SiF_4 density determined using FTIR absorption measurements. (c) Fluorine emission line (704 nm) trend measured simultaneously with direct OES during the experiments (in experimental measurement sequence direct OES data collection started 30 s before the e-beam OES measurements so that time offset has been adjusted). In the 2% area experiment process plasma flicker was observed after 70 s.

In Fig. 6, we show the effect of etch area on the endpoint signals as measured with these optical diagnostics. Three 1.0 μm thick polysilicon wafer samples of sizes of 20.2, 9.7, and 1.6 cm^2, or effective open areas of 25%, 12%, and 2% on a 100 mm wafer, were etched using SF_6 discharge. In all the experiments, the process power and pressure were 200 W and 40 mTorr, respectively. The source to chuck gap was 6 cm. The etch rate as measured with endpoint data shows a decrease with percentage area increase. Atomic fluorine is generally considered to be the etchant in polysilicon etches with SF_6 discharge. Given the high etch rate of silicon with fluorine, it is expected that the etch rate will depend on the area (amount) of material that is etched. This well-known effect based on surface kinetics in etch processes is referred as the loading effect.[32,33] In Fig. 6(b), we have shown density of SiF_4 in the gas phase measured simultaneously during the experiment with FTIR absorbance measurements. Care was taken to synchronize the time between the two measurements. Data points shown in the figure correspond to the mid-point during a 16 s measurement period. It is observed that the SiF_4 densities versus wafer surface area are consistent with the SiF_4 densities measured via e-beam OES. Both density measurements decrease with sample size, as expected. Again, it is noticed that both of the e-beam and FTIR time integrated signals versus area are not consistent with the size ratios. As before, this is likely due to production and loss mechanisms that are heavily influenced by the

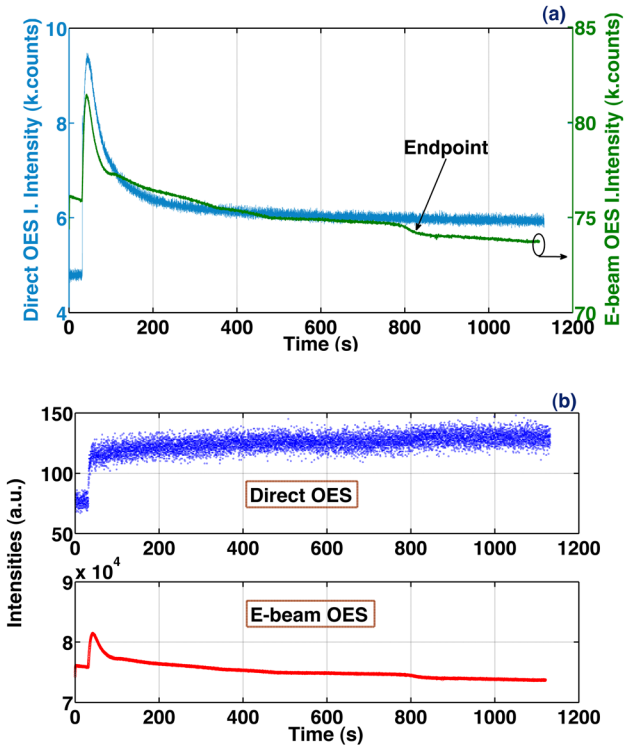

FIG. 7. (Color online) Polysilicon etch process with a 3% sample area and 12 cm gap, 60 W process power and 20 mTorr process pressure. (a) Integrated (290–323 nm) intensity trend as measured with e-beam and direct OES. (b) Endpoint event as sensed in e-beam OES, while the fluorine emission endpoint signature in direct OES is washed out due to poor SNR.

available radicals in the system.[19] In direct OES, Fig. 6(c), the SNR becomes poorer as the percentage area is decreased.

Based on the results from the above studies and other well-known dependence on process parameters (pressure and power), we conducted a process where end point detection with the traditional OES, direct OES, will be challenging task. A 2.4 cm^2 sample, 3% effective open area, at 12 cm source to chuck gap was etched with a SF_6 discharge at 20 mTorr process pressure and 60 W process power, e.g., a low power, remote plasma with a small open area etch. In Fig. 7(a), we show the trend of the 290–323 nm band as measured with direct OES and e-beam OES during the process. While there is a detectable endpoint event in the e-beam OES at about 800 s, it is not detectable with the direct OES. During experiments, samples were loaded into the chamber briefly exposed to atmosphere. So the initial increase in intensity when the process discharge is turned on is likely due to contribution from the classic OH molecular band[34] that is around 308 nm. In Fig. 7(b), the trend of the fluorine 704 nm emission measured with direct OES is shown in comparison to the SiF_4 band from the e-beam. During this experiment, the density of SiF_4 was measured via FTIR to be $6.5 \pm 2 \times 10^{12}\,cm^{-3}$. It is noted that this density is toward the lower limit of sensitivity of the FTIR.

IV. SUMMARY AND CONCLUSIONS

Processes where direct optical emissions are weak pose a challenge to process control, such as endpoint detection. We have presented a comparison endpoint study conducted with direct OES and e-beam OES, a newly developed secondary diagnostic system. We have shown that while emission due to SiF_4 is not excited in process plasma, it is excited in the e-beam diagnostic. Monitoring the SiF_4 band emission during endpoint experiments with SF_6 discharges provided a direct access to one of the primary process effluent in silicon etches through OES. To our knowledge, this is first time such a real time measurement could be made on SiF_4 with OES. Detection capabilities of the diagnostic system in dark plasma process condition have been demonstrated and are consistent with FTIR measurements. Finally, the e-beam results hint at the internal processes occurring in the system. Such internal processes are not examinable with direct OES.

ACKNOWLEDGMENTS

The authors sincerely thank Dr. Gordon Pollack in UTD clean room for his help in sample preparations. The authors thank the funding organizations, NSF (CBET—0922962) and Verity Instruments, Inc., for granting the financial award for this project. Any opinions, findings, and conclusions or recommendations expressed in this material are those of the author(s) and do not necessarily reflect the views of the National Science Foundation.

[1]J. Roland, P. Marcoux, G. Ray, and G. Rankin, J. Vac. Sci. Technol. **3**, 631 (1985).
[2]G. S. Oehrlein, in *Handbook of Plasma Processing Technology*, edited by S. M. Rossnagel, J. J. Cuomo, and W. D. Westwood (Noyes, Park Ridge, NJ, 1990).
[3]S. Qin and H. Yue, "Fault detection and classification for plasma etchers via optical spectroscopy analysis," in *Proceedings of the AIChE Annual Meeting*, 16–21 November 1997.
[4]P. J. Matsuo, B. E. E. Kastenmeier, J. J. Beulens, and G. S. Oehrlein, J. Vac. Sci. Technol. A **15**, 1801 (1997).
[5]P. L. S. Thamban, J. Hosch, and M. J. Goeckner, Rev. Sci. Instrum. **81**, 013502 (2010).
[6]M. J. Goeckner, J. M. Marquis, B. J. Markham, A. K. Jindal, E. A. Joseph, and B.-S. Zhou, Rev. Sci. Instrum. **75**, 884 (2004).
[7]F. Laermer and A. Schilp, German patent DE 4241045 (26 May 1994).
[8]K. M. Eisele, J. Electrochem. Soc. **128**, 123 (1981).
[9]D. J. Oostra, A. Haring, A. E. de Vries, F. H. M. Sanders, and K. Miyake, Appl. Phys. Lett. **46**, 1166 (1985).
[10]A. A. Ayon, R. Braff, C. C. Lin, H. H. Sawin, and M. A. Schmidt, J. Electrochem. Soc. **146**, 339 (1999).
[11]I. W. Rangelow, J. Vac. Sci. Technol. A **21**, 1550 (2003).
[12]S. Gomez, R. J. Belen, M. Kiehlbauch, and E. S. Aydil, J. Vac. Sci. Technol. A **22**, 606 (2004).
[13]L. Tong and K. Nanbu, Vacuum **80**, 1012 (2006).
[14]B. Zhou, E. Joseph,L. J. Overzet, and M. J. Goeckner, J. Vac. Sci. Technol. A **24**, 114 (2006).
[15]E. A. Joseph, B.-S. Zhou, S. P. Sant, L. J. Overzet, and M. J. Goeckner, J. Vac. Sci. Technol. A **26**, 545 (2008).
[16]J. K. Olthhoff and K. E. Greenberg, J. Res. Natl. Inst. Stand. Technol. **100**, 327 (1995).
[17]P. A. Miller, G. A. Hebner, P. D. Pochan, K. E. Greenberg, and B. P. Aragon, J. Res. Natl. Inst. Stand. Technol. **100**, 427 (1995).
[18]J. W. Coburn and M. Chen, J. Appl. Phys. **51**, 3134 (1980).
[19]C. T. Nelson, "Gain and loss mechanisms in fluorocarbon plasmas," Doctoral dissertation (UTD, 2010).
[20]J. D. J. Ingle and S. R. Crouch, *Spectrochemical Analysis* (Prentice Hall, New Jersey, 1988).
[21]Experimental FTIR absorbance measurements were measured as $\log_{10}(I/I_0)$. We have converted to $\ln(I/I_0)$ and thus match Eq. (3).

[22]P. L. S. Thamban, G. Padron-Wells, S. Yun, J. Hosch, and M. J. Goeckner, J. Vac. Sci. Technol. B **30**, 041201 (2012).
[23]D. Z. Cao and D. W. Setser, J. Phys. Chem. **92**, 1169 (1988).
[24]C. Beyer, H. Jenett, and D. Klockow, IEEE Trans. Dielectr. Electr. Insul. **7**, 235 (2000).
[25]M. J. Goeckner, J. A. Meyer, G.-H. Kim, J.-S. Jenq, A. Matthews, J. W. Taylor,and R. A. Breun, J. Vac. Sci. Technol. A **11**, 2543 (1993).
[26]J. F. M. Aarts, Chem. Phys. **101**, 105 (1986).
[27]M. Suto, J. C. Han, L. C. Lee, and T. J. Chuang, J. Chem. Phys. **90**, 2834 (1989).
[28]J. J. Wagner and W. W. Brandt, Plasma Chem. Plasma Process. **1**, 201 (1981).
[29]R. A. Rosenberg, C.-R. Wen, K. Tan, and J.-M. Chen, J. Chem. Phys. **92**, 5196 (1990).
[30]M. Suto, X. Wang, L. C. Lee, and T. J. Chuang, J. Chem. Phys. **86**, 1152 (1987).
[31]H. Biehl, K. J. Boyle, D. P. Seccombe, D. M. Smith, R. P. Tuckett, K. R. Yoxall, H. Baumgartel, and H. W. Jochims, J. Chem. Phys. **107**, 720 (1997).
[32]C. J. Mogab, J. Electrochem. Soc. **124**, 1262 (1977).
[33]M. A. Lieberman and A. J. Lichtenberg, *Principles of Plasma Discharges and Materials Processing*, 2nd ed. (Wiley, New York, 2005).
[34]A. Sarani, A. Y. Nikiforov, and C. Leys, Phys. Plasmas **17**, 063504 (2010).